

Estimation of Ice Cloud Parameters From Ground-Based Infrared Radiometer and Radar Measurements

S. Y. MATROSOV

Cooperative Institute for Research in Environmental Sciences, University of Colorado/NOAA, Boulder

T. UTTAL, J. B. SNIDER, AND R. A. KROPFLI

NOAA Environmental Research Laboratories, Wave Propagation Laboratory, Boulder, Colorado

A technique is presented to estimate ice cloud particle characteristic sizes and concentrations as well as the integrated ice water path from simultaneous ground-based radar and infrared radiometer measurements. The approach is based on the theoretical consideration of infrared thermal radiative transfer within a cloud and can be applied to clouds that are semitransparent in the infrared "window" and horizontally extensive. The suggested technique is applied to radar and infrared radiometer data collected during the Cloud Lidar and Radar Exploratory Test (CLARET-I) experiment. Retrieved values of ice cloud microphysical parameters are in general agreement with results obtained by other methods.

1. INTRODUCTION

Knowing parameters of ice clouds is very important for many climate change studies [Stephens *et al.*, 1990]. The problem of estimating various optical and microphysical parameters of such clouds with different remote sensors both from space and the ground has been addressed in a number of papers [e.g., Intrieri *et al.*, 1991; Parol *et al.*, 1991; Platt *et al.*, 1989; Wu, 1987; Stone *et al.*, 1990]. In this paper we propose a technique to estimate ice cloud particle characteristic sizes and concentrations from simultaneous ground-based radar and infrared radiometer measurements.

Infrared radiometers, operating in the atmospheric "window" of 10–12 μm , are often used to measure the temperature of clouds. However, the measured brightness temperatures coincide with the cloud effective thermodynamic temperatures only if the optical thickness of the emitting clouds is great enough to make them opaque for the radiation at the atmospheric window frequencies. The brightness temperatures of semitransparent clouds, when measured from the ground, are always lower than the thermodynamic temperatures.

Ice clouds (e.g., cirrus clouds) are often optically thin at the infrared window frequencies, even though the imaginary part of the complex refractive index of ice has a local maximal value in this particular wavelength region. Hence the infrared thermal radiation of such clouds depends not only on the temperature distribution within them but also on other cloud parameters. This property of optically thin ice clouds can be used to infer some cloud microphysics characteristics from infrared measurements if the temperature profile is known from radiosonde or other independent data.

This paper shows that cloud optical thickness, which can be obtained from ground-based infrared measurements of downwelling thermal radiation, depends on cloud particle characteristic size and concentration. The two-stream approach for describing the thermal radiation transfer within a

cloud was used to obtain a theoretical basis for the retrieval of these two parameters of cloud microstructure, which are important to different climate and general circulation model studies. However, it is impossible to distinguish the effects on optical thickness of particle sizes from those of concentration using brightness temperature measurements alone.

It is well known that radar reflectivities also depend on the same parameters of cloud microstructure: scatterer size and scatterer concentration. Simple analysis shows that infrared brightness temperatures and radar reflectivities depend in different ways on particle characteristic size and concentration. This fact gives us a means to estimate these parameters of the cloud microstructure from combined ground-based radar/radiometer measurements. However, radiometers, unlike radars, do not give the vertical structure as a function of range, and retrieved values thus refer to the parameters averaged through the cloud.

It is also shown here that we can estimate another important integral parameter of ice clouds, the ice water path (the vertically integrated mass of ice particles per unit area), from combined infrared radiometer and radar measurements.

Simultaneous vertically pointed infrared radiometer and radar measurements were obtained during the Cloud Lidar and Radar Exploratory Test (CLARET) [Eberhard *et al.*, 1990] carried out by NOAA's Wave Propagation Laboratory (WPL). The first part of this research (CLARET-I) took place in the fall of 1989 near Boulder, Colorado, using WPL's Doppler 3.22-cm radar, modified Barnes narrow-angle (2°) infrared radiometer (PRT-5), CO_2 Doppler lidar and microwave radiometer system (working frequencies 90, 31.65, and 20.6 GHz). Radar and infrared radiometer measurements were used to estimate values of ice water path and cloud particle characteristic sizes and concentrations.

2. THEORETICAL CONSIDERATIONS

2.1. The Two-Stream Approximation

Clouds are an important source of the thermal radiation. Radiative transfer within clouds is a complex process involv-

Copyright 1992 by the American Geophysical Union.

Paper number 92JD00968.
0148-0227/92/92JD-00968\$05.00

ing absorption, emission, and multiple scattering of radiation. Using the full integrodifferential radiation transfer equation to describe this process is very laborious and computer intensive. Thus different approximate solutions are widely used [Liou, 1980]. One commonly used approach in the infrared region is the two-stream approximation. All versions of this approximation assume a certain angular distribution of the radiation intensity and are used for plane-parallel models. The general two-stream approximation solutions for upward flux F^\uparrow and downward flux F^\downarrow are [Toon et al., 1989]

$$\begin{aligned} F^\uparrow(\tau) &= k_1 \exp(\Lambda\tau) + \Gamma k_2 \exp(-\Lambda\tau) + C^\uparrow(\tau) \\ F^\downarrow(\tau) &= \Gamma k_1 \exp(\Lambda\tau) + k_2 \exp(-\Lambda\tau) + C^\downarrow(\tau), \end{aligned} \quad (1)$$

where τ is the optical thickness within the cloud increasing from the top to the bottom, $C^\downarrow(\tau)$ and $C^\uparrow(\tau)$ describe the thermal source, the coefficients k_1 and k_2 are determined by boundary conditions, and the coefficients Λ and Γ can be expressed in terms of γ_1 and γ_2 :

$$\begin{aligned} \Lambda &= (\gamma_1^2 - \gamma_2^2)^{1/2} \\ \Gamma &= \gamma_2 / (\gamma_1 + \Lambda). \end{aligned} \quad (2)$$

where γ_1 and γ_2 depend on a particular version of the two-stream approximation. For the quadrature two-stream approximation used here,

$$\begin{aligned} \gamma_1 &= 0.866[2 - \omega(1 + g)] \\ \gamma_2 &= 0.866\omega(1 - g), \end{aligned} \quad (3)$$

where ω and g are the single scattering albedo and the scattering asymmetry parameter, respectively. The intensities of the upwelling and downwelling radiations [$I^{\uparrow(\downarrow)}(\tau)$] within the cloud can be estimated from

$$F^{\uparrow(\downarrow)}(\tau) = 2\pi\mu_1 I^{\uparrow(\downarrow)}(\tau), \quad (4)$$

where μ_1 is the mean value of the zenith angle cosine. In the quadrature version of the two-stream approximation model, $\mu_1 = 0.577$.

The thermal source terms can be shown to be [Toon et al., 1989]

$$\begin{aligned} C^\uparrow(\tau) &= 2\pi\mu_1 \{B_0 + B_1[\tau + 1/(\gamma_1 + \gamma_2)]\} \\ C^\downarrow(\tau) &= 2\pi\mu_1 \{B_0 + B_1[\tau - 1/(\gamma_1 + \gamma_2)]\}, \end{aligned} \quad (5)$$

where $B_0 = B(T_t)$, $B_1 = [B(T_{bt}) - B(T_t)]/\tau_0$, $B(\)$ is the Planck function, and T_t and T_{bt} are the temperatures of the cloud top and bottom, respectively. The optical thickness τ_0 of a vertically homogeneous cloud is related to its geometrical thickness H_c by means of the extinction coefficient, $\alpha_e(\tau_0) = \alpha_e H_c$.

2.2. Boundary Conditions

We assume ice clouds to be vertically homogeneous and horizontally infinite. We also assume, after Platt and Dillely [1979], that the infrared radiation of gaseous constituents of the atmosphere above and within the cirrus clouds can be neglected in comparison with the radiation of the clouds themselves. However, we account for the radiation and transmittance of the atmosphere below the cloud bottom. In

this case, the boundary conditions at the top ($\tau = 0$) and at the bottom ($\tau = \tau_0$) of a cloud are

$$F^\downarrow(0) = 0 \quad (6)$$

$$F^\uparrow(\tau_0) = 2\pi\mu_1 B(T_s)P_a + 2\pi\mu_1 I_a^\uparrow,$$

where T_s is the underlying surface temperature, P_a is the transmittance of atmosphere between the cloud bottom and the ground, and I_a^\uparrow is the upwelling radiation intensity of the atmosphere between the ground and the cloud bottom.

In our model calculations, we are primarily interested in the brightness temperatures of the downwelling infrared radiation. At the cloud bottom level, these temperatures (T_{bc}^\downarrow) can be obtained from the downwelling intensities:

$$I^\downarrow(\tau_0) = B(T_{bc}^\downarrow). \quad (7)$$

However, intensities I_g^\downarrow (or brightness temperatures T_{bg}^\downarrow) measured at the ground differ from those at the cloud bottom level. The corresponding relationship is given by

$$I_g^\downarrow = I_c^\downarrow P_a + I_a^\downarrow, \quad (8)$$

where I_a^\downarrow is the ground level thermal radiation intensity of the atmosphere, τ_a is the optical thickness of the atmosphere confined between the cloud bottom and the ground, and $I_c^\downarrow \equiv I^\downarrow(\tau_0)$. The equations for I_a^\uparrow , which appears in the boundary conditions (6), and I_a^\downarrow are

$$I_a^\uparrow = \int_0^{\tau_a} B[T(\tau)] \exp[-(\tau_a - \tau)] d\tau \quad (9)$$

$$I_a^\downarrow = \int_0^{\tau_a} B[T(\tau)] \exp(-\tau) d\tau, \quad (10)$$

where $T(\tau)$ is the air temperature. Using the mean value theorem, one can obtain

$$I_a^\uparrow = B(T^*)(1 - P_a) \quad (11)$$

$$I_a^\downarrow = B(T^{**})(1 - P_a), \quad (12)$$

where $P_a \equiv \exp(-\tau_a)$ and T^* and T^{**} are the effective temperatures of the atmosphere for the upwelling and downwelling radiation, respectively.

We performed numerical modeling of I_a^\uparrow and I_a^\downarrow for typical values of P_a ranging from 0.7 to 0.9 [Platt and Dillely, 1979] using (9) and (10) and assuming that the absorption of the atmosphere at the window frequencies is mostly due to the water vapor. In this case, $d\tau = \alpha_w(h) dh$, where α_w is the volume water vapor absorption coefficient and h is the vertical coordinate. The vertical profile of α_w can be assumed to be exponential:

$$\alpha_w(h) = \alpha_w(0) \exp(-h/h_w), \quad (13)$$

where h_w is the water vapor scale height. Usually $h_w \approx 2$ km [Khragian, 1978].

Model calculations using the linear temperature gradient showed that $T^* \approx T^{**}$ within an accuracy of about 1.5 K and also that the effective temperatures do not significantly depend on atmospheric transmittance P_a if $P_a \geq 0.75$. Depending on the cloud bottom height, T^* and T^{**} are equal to the air temperature at altitudes of 1.1–1.4 km. A more

accurate estimation of T^* and T^{**} can be made for every particular case of cloud bottom height and the temperature and water vapor stratifications.

2.3. Microphysical and Observational Parameters of a Cloud

Cirrus cloud particles were modeled as solid ice spheres with diameters varying from 5 μm to 2 mm. A review of the literature on cirrus cloud microstructure was made by *Dowling and Radke* [1990], who showed that ice particle size probability density functions usually have a single peak with respect to particle diameter. This implies that description of ice particle size distribution by a simple exponential function, $N(D) = N_0 \exp(-bD)$, is inadequate, so in this work we used the first-order gamma distribution:

$$N(D) = N_0 D \exp(-4.67D/D_m), \quad (14)$$

which meets the requirement for a single peak with respect to the particle diameter. D_m is the median diameter, which splits the distribution into two equal volume parts. The median diameter for this type of distribution is approximately 2.3 times greater than the mean diameter D_0 if D_0 is defined in the following usual way:

$$D_0 = \int_{D_{\min}}^{D_{\max}} DN(D) dD / \int_{D_{\min}}^{D_{\max}} N(D) dD, \quad (15)$$

Figure 1 shows the extinction efficiency, single scattering albedo, and asymmetry factor for an ice particle computed using the Mie theory (for details see, e.g., *Bohren and Huffman* [1983]). All optical characteristics shown here were computed for a wavelength of 11 μm , which is in the middle of the window region of interest. The complex refractive index of ice at this wavelength, $m = 1.0925 + i0.248$, was adapted from *Warren* [1984]. It can be seen from Figure 1 that all three characteristics are close to their asymptotic values when $D \geq 20 \mu\text{m}$. These values are 2 for the extinction efficiency, 1 for the asymmetry factor, and 0.5 for the single scattering albedo. This result suggests a means for an efficient calculation of different optical characteristics of ice clouds at window frequencies, thus avoiding the labori-

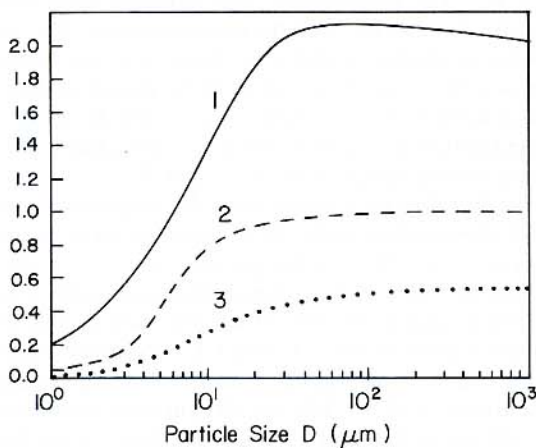


Fig. 1. Curve 1, ice sphere extinction efficiency; curve 2, asymmetry factor; and curve 3, single scattering albedo as a function of particle diameter at $\lambda = 11 \mu\text{m}$.

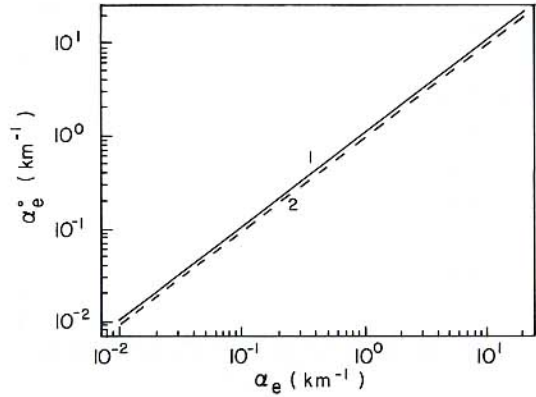


Fig. 2. Comparison of ice particle extinction coefficients calculated by using the Mie theory, α_e , and those calculated using (17), α_e^0 . Curve 1, $D_m = 20 \mu\text{m}$; curve 2, $D_m = 500 \mu\text{m}$.

ous computations inherent in the Mie theory. For the extinction coefficient, the corresponding simple equation will be

$$\alpha_e^0 = (\pi/2) \int_{D_{\min}}^{D_{\max}} D^2 N(D) dD. \quad (16)$$

Our computational analysis shows that using zero and infinity as the integral limits instead of $D_{\min} = 5 \mu\text{m}$ and $D_{\max} = 2 \text{mm}$ produces changes in α_e^0 of only a few percent when the median particle size D_m varies from 20 to 600 μm . Taking the integral (16) from zero to ∞ results in a straightforward equation for α_e^0 :

$$\alpha_e^0 \approx 0.02 N_0 D_m^4 \text{ cm}^{-1}. \quad (17)$$

Figure 2 shows the comparison of the extinction coefficients calculated using the Mie theory (α_e) and from (17) (α_e^0) for two different cloud particle median sizes ($D_m = 20 \mu\text{m}$ and $D_m = 500 \mu\text{m}$). For $D_m = 20 \mu\text{m}$, the difference between α_e and α_e^0 is about 8%; however, it swiftly diminishes as D_m increases. For $D_m = 500 \mu\text{m}$, it is less than 2%.

In a similar manner we can obtain simple equations for radar reflectivity Z_i , cloud ice mass content w_i , and cloud particle concentration C_0 :

$$Z_i = \int_0^\infty D^6 N(D) dD \approx 0.0223 N_0 D_m^8 = 0.487 C_0 D_m^6 \text{ cm}^3 \quad (18)$$

$$w_i = (\pi/6) \rho_i \int_0^\infty D^3 N(D) dD \approx 5090 N_0 D_m^5 = 1.11 \times 10^5 C_0 D_m^3 \text{ g m}^{-3} \quad (19)$$

$$C_0 = \int_0^\infty N(D) dD \approx 0.0458 N_0 D_m^2 \text{ cm}^{-3}, \quad (20)$$

where N_0 is in cm^{-5} , D_m is in centimeters, and the ice density ρ_i is assumed to be 0.9 g cm^{-3} .

Comparing (17) and (19) shows that the specific extinction coefficient behaves as D_m^{-1} . This is illustrated by Figure 3, where however, the specific extinction coefficients were calculated using the Mie theory.

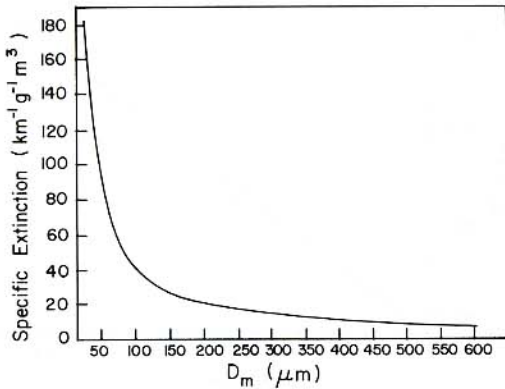


Fig. 3. Specific extinction coefficient in ice clouds as a function of ice particle median size D_m at $\lambda = 11 \mu\text{m}$.

3. RESULTS OF MODEL CALCULATIONS

3.1. Input Parameters

Downwelling radiation fluxes were calculated using the quadrature two-stream approximation described above. These fluxes were then converted into brightness temperatures using (4) and (7). The input conditions were taken from the averages for a 2-hour cloudy period on October 4, 1989, during the CLARET-I experiment, when simultaneous vertically pointed radar and infrared radiometer measurements were performed. Between 1900 and 2100 UTC the observed cirrus cloud was semitransparent in the window region and horizontally extended with relatively stable top and bottom heights. Figure 4 shows the cloud bottom and cloud top heights over time as determined by the radar. During gaps in the data shown, the radar performed another type of measurements.

This case was unique because even though the cloud had almost stable geometrical boundaries for more than 2 hours, a broad range of infrared brightness temperatures and radar reflectivities was observed. The brightness temperatures of the downwelling infrared radiation measured by the modified WPL PRT-5 radiometer varied from 206 to 255 K and were significantly colder than the thermodynamic cloud bottom temperature measured by radiosonde. Knowing the vertical

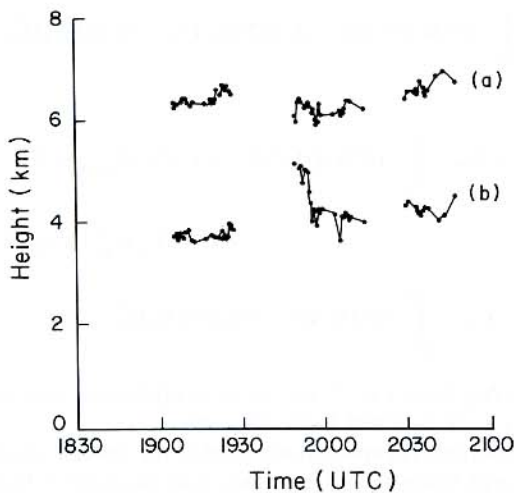


Fig. 4. Time dependencies of (a) cloud top and (b) cloud bottom heights at the experimental site on October 4, 1989.

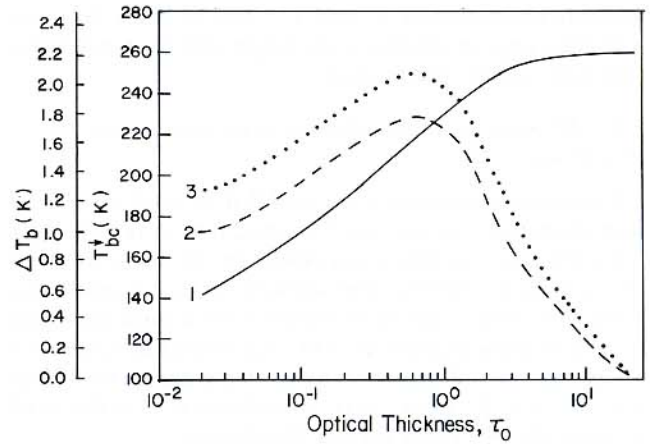


Fig. 5. Brightness temperatures T_{bc}^{\downarrow} and brightness temperature differences ΔT_b versus ice cloud optical thickness at different particle median sizes. Curve 1, $T_{bc}^{\downarrow}(D_m = 40 \mu\text{m})$; curve 2, $\Delta T_b = T_{bc}^{\downarrow}(D_m = 40 \mu\text{m}) - T_{bc}^{\downarrow}(D_m = 300 \mu\text{m})$; and curve 3, $\Delta T_b = T_{bc}^{\downarrow}(D_m = 40 \mu\text{m}) - T_{bc}^{\downarrow}(D_m = 600 \mu\text{m})$.

temperature and humidity profiles from the same data, we found the effective temperatures of the atmosphere to be $T^* \approx T^{**} \approx 283 \text{ K}$.

At 1928 UTC the cloud radar echo became very weak for several minutes. This almost clear sky interval gave us the opportunity to estimate the atmospheric radiation I_a^{\downarrow} and therefore the atmospheric transmittance P_a from (12). The brightness temperature T_{ba}^{\downarrow} corresponding to I_a^{\downarrow} was about 199 K, and the P_a was found to be 0.87. Vertically averaged radar reflectivities Z_e inside the cloud were in the interval from about -19 to -5 dBZ . The measured equivalent water radar reflectivity Z_e relates to the equivalent ice radar reflectivity for spherical particles Z_i introduced in (18) in the following way:

$$Z_i = \left| \frac{m_w^2 - 1}{m_w^2 + 2} \right|^2 \left| \frac{m_i^2 + 2}{m_i^2 - 1} \right|^2 Z_e \approx 5.3 Z_e, \quad (21)$$

where m_w and m_i are the complex refractive indices of water and ice, respectively, at the radar wavelength ($\lambda = 3.2 \text{ cm}$).

Temperatures at cloud altitudes were estimated from National Weather Service radiosonde launches at 1100 and 2300 UTC. The radiosondes were released from Denver, Colorado, about 30 km from the remote sensors. The vertical temperature profile within the cloud was approximately stationary. We used these values in the model calculations: mean cloud bottom temperature $T_{bt} = 260 \text{ K}$, mean cloud top temperature $T_t = 245 \text{ K}$, mean cloud thickness $H = 2.5 \text{ km}$, and surface temperature $T_s = 291 \text{ K}$.

Curve 1 in Figure 5 shows how the brightness temperatures of downwelling radiation T_{bc}^{\downarrow} depend on cloud optical thickness τ_0 for the median particle size $D_m = 40 \mu\text{m}$. Calculations represent averaged radiation values in the wavelength region of $9.95\text{--}11.43 \mu\text{m}$, where the PRT-5 radiometer used in the CLARET-I experiment operated. Curves 2 and 3 in Figure 5 show how the brightness temperatures for $D_m = 300$ and $600 \mu\text{m}$ differ from those for $D_m = 40 \mu\text{m}$ at the same values of τ_0 . One can see that the differences are less than 2 K for this considerably large range of characteristic size parameter variation. This implies that the brightness temperatures of the downwelling radiation are

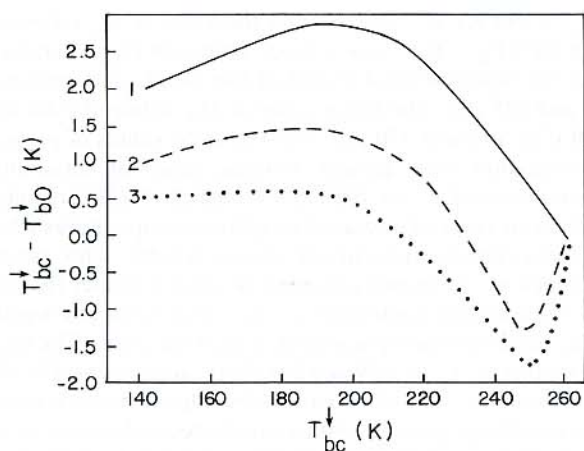


Fig. 6. Differences between brightness temperatures obtained from the two-stream model T_{bc}^{\downarrow} and from (22) T_{b0}^{\downarrow} for different particle median sizes. Curve 1, $D_m = 40 \mu\text{m}$; curve 2, $D_m = 300 \mu\text{m}$; and curve 3, $D_m = 600 \mu\text{m}$.

primarily determined by the cloud optical thickness; however, for different median sizes D_m , different particle concentrations are necessary to maintain a fixed value of the optical thickness.

3.2. Technique for Cloud Parameter Estimation

One can see that the brightness temperature of the downwelling radiation at the cloud bottom level (curve 1 in Figure 5) asymptotically approaches the thermodynamic temperature of the cloud bottom as the optical thickness τ_0 increases. This suggests a method to match the brightness temperature curves using a simple exponential function:

$$B(T_{b0}^{\downarrow}) = B(T_{bt})[1 - \exp(-a_0\tau^0)], \quad (22)$$

where

$$\tau^0 = \alpha_e^0 H_c \quad (23)$$

and the Planck function B is calculated at a wavelength of $10.7 \mu\text{m}$, which is the middle of the PRT-5 radiometer wavelength band.

It can be easily shown that for a predominantly absorbing medium, $a_0 \approx 1$. From the statistical analysis of results obtained from the two-stream approximation model and from (22), we found that for our case, when volume scattering processes are as important as absorption, the best fit value for the coefficient a_0 in (22) is 0.7. Figure 6 shows the differences between the model brightness temperatures T_{bc}^{\downarrow} and those, T_{b0}^{\downarrow} , calculated from (22) using (17) and (23). The differences are within the range $\pm 3 \text{ K}$ for the wide range of values assigned to D_m . We note also that though (22) was obtained for a particular temperature profile, it is generally valid for a broader range of meteorological conditions.

It was established that different versions of the two-stream approximation (e.g., the Eddington and the hemispheric mean versions) give brightness temperature values that can differ by 2–3 K from those obtained here, using the quadrature two-stream approximation. Considering this fact, one can assume that the very simple equation (22) can be successfully used for estimating the brightness temperatures

of downwelling radiation of ice clouds in the wavelength region $9.95\text{--}11.43 \mu\text{m}$.

The simplicity of (22) also gives us an opportunity to estimate the optical thickness of a semitransparent ice cloud in a very simple way if the cloud brightness and thermodynamic temperatures are known. If we also know the geometrical cloud thickness H_c , we can estimate the product of the cloud particle distribution parameter N_0 and the median particle size D_m raised to the fourth power from (17):

$$N_0 D_m^4 = -72 \ln [1 - B(T_{bc}^{\downarrow})/B(T_{bt})]/H_c, \quad (24a)$$

or in terms of the median particle size and concentration

$$C_0 D_m^2 = -3.3 \ln [1 - B(T_{bc}^{\downarrow})/B(T_{bt})]/H_c, \quad (24b)$$

where the brightness temperature at the cloud bottom level T_{bc}^{\downarrow} is obtained from the brightness temperature measurements at the ground level T_{b0}^{\downarrow} in the following way:

$$B(T_{bc}^{\downarrow}) = [B(T_{bg}^{\downarrow}) - B(T_{ba}^{\downarrow})(1 - P_a)]/P_a. \quad (25)$$

If infrared measurements of the clear sky are not available, the brightness temperature of the atmospheric thermal radiation T_{ba}^{\downarrow} and the atmosphere transmittance P_a can be estimated a priori from data about the water vapor content in the atmosphere. For (23), we assumed vertical homogeneity of the cloud microstructure parameters; otherwise retrieved from the brightness temperatures product, $N_0 D_m^4$ (or $C_0 D_m^2$) refers to the effective values characterizing the whole cloud layer.

As shown above, infrared brightness temperatures measured at the ground respond to the cloud optical thickness, and it is impossible to distinguish between the effects of particle sizes and those of concentration. However, as seen from (18), the radar reflectivities also depend on the combination of N_0 and D_m . By combining measurements of radar reflectivity and infrared brightness temperatures, we can estimate the vertically averaged cloud particle median size:

$$D_m \approx 1.35 \{-\bar{Z}_e H_c / \ln [1 - B(T_{bc}^{\downarrow})/B(T_{bt})]\}^{0.25}, \quad (26)$$

where the overbar means the value of radar reflectivity averaged through the cloud thickness. From (20) and (24a), one can obtain the corresponding value of particle concentration, C_0 .

Equation (26) obtained from (18) and (24b) implies the spherical model for cirrus particles. A nonspherical particle with a horizontally oriented major dimension will give somewhat stronger backscatter echo than that of an equivalent-volume sphere if the radar is pointing vertically. This will lead to overestimation of product $C_0 D_m^6$. At the same time, particle geometrical cross sections which are proportional to their extinction cross sections will also be greater. This will result in an overestimation of product $C_0 D_m^2$. Both these overestimation effects will partially cancel out when estimating the median particle size from (26). However, we acknowledge that careful consideration of nonspherical effects is an important topic of future research.

4. EXPERIMENTAL EXAMPLE OF CIRRUS CLOUD PARAMETER DETERMINATION

4.1. Particle Sizes and Concentrations

The cirrus cloud measurements taken on October 4, 1989, during CLARET-I were chosen to illustrate the technique

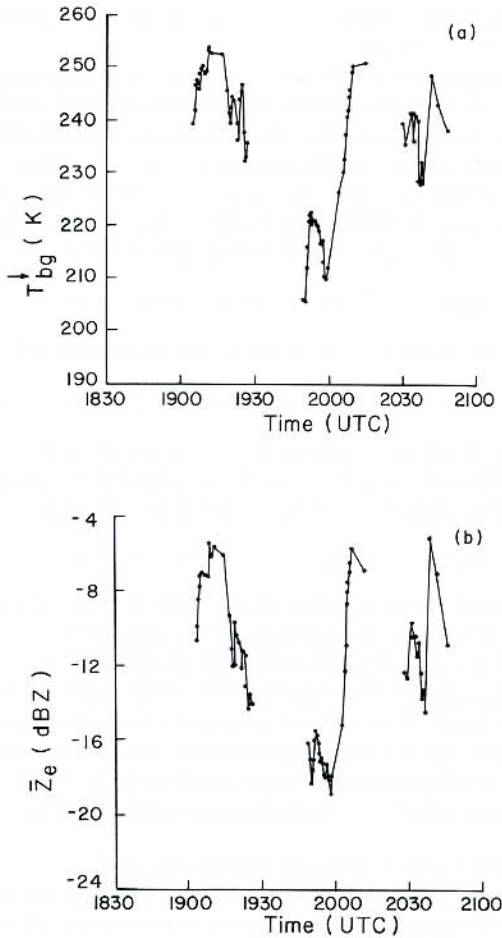


Fig. 7. Time dependencies of (a) measured brightness temperatures T_{bg}^{\downarrow} and (b) circular polarization radar reflectivities Z_e averaged through the cloud during CLARET-I on October 4, 1989.

suggested here for determining ice cloud particle sizes and concentrations. Figure 4 shows the geometrical boundaries of the observed cirrus cloud. The brightness temperatures of the downwelling radiation measured by the infrared radiometer and the radar reflectivities vertically averaged through the cloud thickness are shown in Figures 7a and 7b, respectively. Radar reflectivities were also averaged in 30-s intervals.

The number of experimental points collected between 1900 and 2100 UTC for the following analysis was 75. These points corresponded to the pure ice phase cloud particle case. A number of points between 2006 and 2030 UTC were excluded from the analysis because the collocated microwave radiometer [Hogg *et al.*, 1983] indicated the presence of liquid water in the cloud.

Regions of higher values of T_{bg}^{\downarrow} and Z_e (e.g., between 1900 and 1927 UTC and between 2010 and 2048 UTC) corresponded to more dense cloud with the optical thickness τ_0 from 0.6 to 1.9 as determined from (22) and the information about the atmospheric transmittance. The region of lower values of T_{bg}^{\downarrow} and Z_e (between 1950 and 2006 UTC) corresponded to more transparent cloud with τ_0 from 0.1 to 0.6.

Figures 8a and 8b show the vertically averaged particle median sizes D_m and concentrations C_0 retrieved using (25), (26), and (20), where actual measured values of T_{bg}^{\downarrow} , T_{ba}^{\downarrow}

($T_{ba}^{\downarrow} = 199$ K), Z_e , and H_c and the value of P_a estimated from (12) ($P_a = 0.87$) were used. Values of D_m , characterizing the whole vertical extent of the cloud, vary between 125 and 225 μm . The mean value of D_m between 1900 and 2100 UTC is about 170 μm . The retrieved values of particle concentration show greater dynamic range of variability. The maxima of C_0 at 1925, 1953, and 2015 UTC resulted from the increase of measured brightness temperatures when the radar reflectivities did not change notably. This can be explained by the growing number of small particles that did not considerably contribute to the radar echo but significantly increased the optical thickness of the cloud. The local maxima of D_m at 1959 and 2042 UTC accompanied by the minima of C_0 could be caused by a local increase in the fraction of large particles with a simultaneous decrease in the total particle concentration, resulting in the reflectivity peak and the decline of the brightness temperatures.

Realizing that the measurements of clear-sky radiation with the PRT-5 infrared radiometer are subject to possible errors [Shaw, 1991], we performed the retrieval process with a theoretically estimated colder value of $T_{ba}^{\downarrow} = 193$ K ($P_a = 0.9$). As a result, the mean value of D_m decreased by 5%, and the mean value of C_0 increased by 18%. These variations of retrieved parameters due to changes in the back-

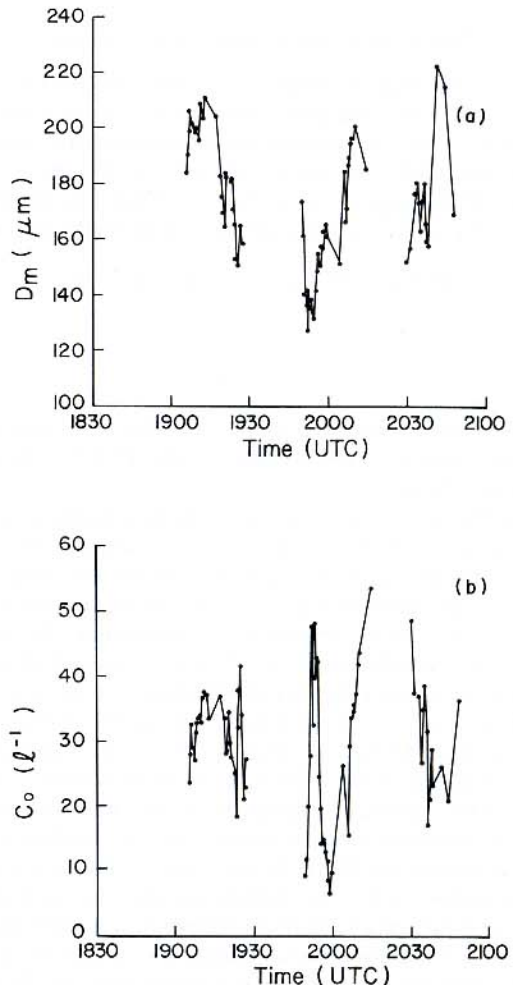


Fig. 8. Time dependencies of (a) retrieved particle median size D_m and (b) concentration C_0 during CLARET-I on October 4, 1989.

ground sky radiation are relatively small because, for this experimental case, the cloud thermal radiation was of sufficiently greater intensity than that of the sky.

The retrieved particle median sizes are within a reasonable range for cirrus cloud particles [Pruppacher and Klett, 1978; Dowling and Radke, 1990]. Unfortunately, there were no in situ aircraft measurements that could be compared to the obtained data. However, we can compare our particle size data to values obtained from the same experimental case using another technique based on the comparison of lidar and radar backscattering coefficients [Intrieri et al., 1991]. This technique gives for the effective radii of cloud particles values from 70 to 190 μm for the same experimental case. The effective radius is defined as [Hansen and Travis, 1974]

$$r_{\text{eff}} = \int_0^\infty r^3 N(r) dr / \int_0^\infty r^2 N(r) dr. \quad (27)$$

When the particle size distribution is the gamma function of the first order, $r_{\text{eff}} \approx 0.43D_m$, and thus the sizes reported by Intrieri et al. [1991] are in reasonable agreement with ours. This agreement is encouraging because the quantitatively similar results were obtained by different techniques.

4.2. Estimation of Ice Water Path

One of the important parameters in cloud microstructure is ice mass content w_i (see (19)) and its path integral, usually called the ice water path (IWP):

$$\text{IWP} = \int w_i(h) dh, \quad (28)$$

where the integration is carried out over the vertical extent of a cloud.

Knowing the particle median size within the cloud D_m and the particle concentration C_0 as a result of the retrieval, and knowing the cloud thickness H_c from the direct radar measurements, we can estimate IWP using (19). The IWP values were retrieved for all 75 experimental points with their individual measurements of T_{bg}^\downarrow , Z_e , and H_c . As before, we assumed that the cloud was vertically homogeneous and the atmospheric brightness temperature T_{ba}^\downarrow and the atmospheric transmittance P_a^\downarrow remained constant for the whole period of observations ($T_{ba}^\downarrow = 199 \text{ K}$ and $P_a = 0.87$).

Figure 9 shows IWP data retrieved by the proposed technique and those (IWP_s) obtained from the empirical equation derived by Sassen [1987]:

$$w_i = 0.037Z_i^{0.696}. \quad (29)$$

This equation, obtained as a result of analyzing experimental data, relates the radar reflectivity and the ice mass content of ice clouds.

One can see from Figure 9 that both techniques give very close results. The average values of ice water path obtained by our technique and Sassen's equation for the period from 1900 to 2100 UTC are 42.7 and 47.4 g m^{-2} , respectively. The correlation coefficient between IWP and IWP_s is about 0.9. The agreement is surprisingly good, given the fact that our technique uses the individual values of particles' characteristic sizes and concentrations to obtain IWP, in contrast with (29), which is an empirical relationship. We can anticipate many other experimental situations where agreement will

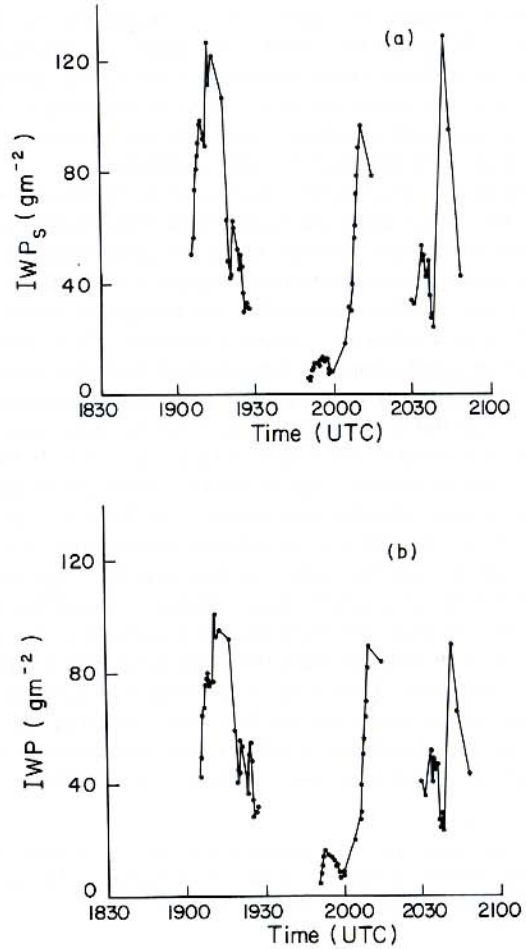


Fig. 9. Time dependencies of ice water path retrieved (a) using the empirical equation by Sassen [1987] and (b) by the proposed technique.

not be so good because (29) represents only an average relationship without taking into consideration independent changes in particle sizes and concentrations.

We also performed the sensitivity analysis, which showed that errors in the brightness temperature measurements (or errors in estimation of the cloud bottom temperature) of 3 K could cause errors of the retrieved particle median sizes, concentrations, and IWP of about 8%, 25%, and 11%, respectively. The 2-dB errors in radar reflectivity measurements could result in uncertainty of D_m , C_0 , and IWP of about 12%, 25%, and 12%, respectively.

5. CONCLUDING REMARKS

In this paper we proposed a technique to estimate the characteristic sizes and concentrations of ice cloud particles from the combined ground-based measurements of downwelling infrared thermal radiation and radar reflectivities. The technique is based on a theoretical consideration of cloud thermal emission and reflectance and can be applied to horizontally extended ice clouds that are semitransparent at the infrared window frequencies. The radiation correction for atmospheric water vapor can be done either by measuring clear-sky brightness temperatures or theoretically from the radiosonde or microwave radiometer data.

This technique also allows us to estimate the integral ice water path within the cloud. The suggested approach was applied to process a data set obtained during one experimental period. The retrieved values of ice cloud particle characteristic sizes and cloud ice water path are in general agreement with data obtained by other methods.

Among the uncertainties inherent to our technique, we can name the approximate character of the two-stream radiation transfer model and assumptions made concerning the shape of particle size distribution and sphericity of particles. Consideration of effects caused by the nonsphericity of cirrus cloud particles deserves separate research. To estimate the extinction coefficients for nonspherical particles using (16), we will have to use more realistic geometrical cross sections rather than those of spheres. Likewise, we have to account for particle shapes when considering radar reflectivities. In theory, the technique suggested in this paper can be adjusted to the case of nonspherical particles if in the basic equations (16)–(19) we use different modified characteristics of particle sizes rather than the same median size D_m . Leaving the detailed study of particle shape influences for further investigations, we only note here that characteristics of scatterer shapes can be inferred from the radar polarization measurements [Matrosov, 1991a, b]. Experimentally, particle shape characteristics could be studied with the WPL Ka-band radar upgraded with a new offset Cassegrain antenna having good polarization properties [Kropfli et al., 1990].

Acknowledgments. The research was funded, in part, by the U.S. Department of Energy's Atmospheric Radiation Measurement Program under grant DE-AI06-91RL12089.

REFERENCES

- Bohren, C. F., and D. R. Huffman, *Absorption and Scattering of Light by Small Particles*, John Wiley, New York, 1983.
- Dowling, D. R., and L. F. Radke, A summary of the physical properties of cirrus clouds, *J. Appl. Meteorol.*, **29**, 970–978, 1990.
- Eberhard, W. L., T. Uttal, J. M. Intrieri, and R. J. Willis, Cloud parameters from IR lidar and other instruments: CLARET design and preliminary results, in *Proceedings of the Seventh Conference on Atmospheric Radiation*, pp. 343–348, American Meteorological Society, Boston, Mass., 1990.
- Hansen, J. E., and L. D. Travis, Light scattering in planetary atmospheres, *Space Sci. Rev.*, **16**, 527–610, 1974.
- Hogg, D. C., F. O. Guiraud, J. B. Snider, M. T. Decker, and E. R. Westwater, A steerable dual-channel microwave radiometer for measurement of water vapor and liquid in the troposphere, *J. Appl. Meteorol.*, **22**, 789–806, 1983.
- Intrieri, J. M., W. L. Eberhard, and T. Uttal, Determination of cirrus cloud particle effective radii using radar and lidar backscattering data, in *Proceedings of the 25th Conference on Radar Meteorology*, pp. 809–812, American Meteorological Society, Boston, Mass., 1991.
- Khrgian, A. K., *Atmospheric Physics* (in Russian), Gidrometeoizdat, Leningrad, 1978.
- Kropfli, R. A., B. W. Bartram, and S. Y. Matrosov, The upgraded WPL dual-polarization 8-mm wavelength Doppler radar for microphysical and climate research, in *Proceedings of the Conference on Cloud Physics*, pp. 341–345, American Meteorological Society, Boston, Mass., 1990.
- Liou, K. N., *An Introduction to Atmospheric Radiation*, Academic, San Diego, Calif., 1980.
- Matrosov, S. Y., Theoretical study of radar polarization parameters obtained from cirrus clouds, *J. Atmos. Sci.*, **48**, 1062–1070, 1991a.
- Matrosov, S. Y., Prospects for the measurement of ice cloud particle shape and orientation with elliptically polarized radar signals, *Radio Sci.*, **26**, 847–856, 1991b.
- Parol, F., J. C. Buriez, G. Brogniez, and Y. Fouquart, Information content of AVHRR channel 4 and 5 with respect to the effective radius of cirrus cloud particles, *J. Appl. Meteorol.*, **30**, 973–984, 1991.
- Platt, C. M. R., and A. C. Dilley, Remote sensing of high clouds, II, Emissivity of cirrostratus, *J. Appl. Meteorol.*, **18**, 1144–1150, 1979.
- Platt, C. M. R., J. D. Spinhirne, and W. D. Hart, Optical and microphysical properties of a cold cirrus cloud: Evidence for regions of small ice particles, *J. Geophys. Res.*, **94**, 11,151–11,164, 1989.
- Pruppacher, H. R., and J. D. Klett, *Microphysics of Clouds and Precipitation*, D. Reidel, Hingham, Mass., 1978.
- Sassen, K., Ice cloud content from radar reflectivity, *J. Clim. Appl. Meteorol.*, **26**, 1050–1053, 1987.
- Shaw, J. A., Calibration of infrared radiometers for cloud-base temperature remote sensing: Technique and error analysis, *NOAA Tech. Memo. ERL WPL-207*, Natl. Oceanic and Atmos. Admin., Washington, D. C., 1991.
- Stephens, G. L., S. C. Tsay, P. W. Stackhouse, Jr., and P. J. Flatau, The relevance of the microphysical and radiative properties of cirrus clouds to climate and climatic feedback, *J. Atmos. Sci.*, **47**, 1742–1753, 1990.
- Stone, R. S., G. L. Stephens, C. M. R. Platt, and S. Banks, The remote sensing of thin cirrus cloud using satellites, lidar and radiative transfer theory, *J. Appl. Meteorol.*, **29**, 353–366, 1990.
- Toon, O. B., C. P. McKay, T. P. Ackerman, and K. Santhanam, Rapid calculation of radiative heating rates and photodissociation rates in inhomogeneous multiple scattering atmospheres, *J. Geophys. Res.*, **94**, 16,287–16,301, 1989.
- Warren, S. G., Optical constants of ice from the ultraviolet to the microwave, *Appl. Opt.*, **23**, 1206–1225, 1984.
- Wu, M. L. C., Determination of ice cloud water content and geometrical thickness using microwave and infrared radiometric measurements, *J. Clim. Appl. Meteorol.*, **26**, 878–884, 1987.
- R. A. Kropfli, J. B. Snider, and T. Uttal, NOAA\ERL, Wave Propagation Laboratory, Boulder, CO 80303.
- S. Y. Matrosov, Cooperative Institute for Research in Environmental Sciences, University of Colorado, R/E/WP6, 325 Broadway, Boulder, CO 80303-3328.

(Received September 17, 1991;
revised April 16, 1992;
accepted April 22, 1992.)